Journal of Low Temperature Physics, Vol. 55, Nos. 1/2, 1984

Magnetic Coupling of ^{3}He with a Fluorocarbon Substrate

L. J. Friedman, T. J. Gramila, and R. C. Richardson

Laboratory of Atomic and Solid State Physics and the Materials Science Center, Cornell University, Ithaca, New York

(Received September 12, 1983)

We observe a nuclear interaction between ^{3}He and the ^{19}F spin species of a fluorocarbon substrate. The magnetization of a ^{3}He film is strongly linked to that of the ^{19}F substrate spins. We use this interaction as a probe of the ^{3}He to identify several features important in surface relaxation.

1. INTRODUCTION

The nature of ^{3}He surface interactions has been of interest to low-temperature physicists for some time. Starting in the late 1950s,[1–3] experiments designed to measure magnetic properties of bulk ^{3}He liquid revealed several irregularities due to surface influences. Although wall effects were initially viewed as an annoyance, some later experiments[4–7] specifically sought to study ^{3}He properties in confined geometries. Using a variety of substrates with pore sizes ranging from 10 to 10^3 Å, these NMR experiments recorded both the temperature and field dependence for the ^{3}He T_1 and T_2. With such large surface areas in contact with the ^{3}He liquid, wall effects are of course dominant. One of the more prominent features of such work is that the ^{3}He T_1 is typically hundreds of milliseconds rather than the hundreds of seconds measured for the bulk experiments. This T_1 is observed to increase linearly with the applied H_0 field, and displays a broad maximum around 0.4 K as the temperature varies. Although the time scale for these T_1 values changes somewhat with different substrates, the qualitative temperature and field dependences appear to be a characteristic aspect of the surface relaxation. Thus, despite the lack of substrate characterization, there appears to be some (as yet unrecognized) common thread underlying the physics. One interesting attempt[8] to account for the linear field dependence of T_1 (without provision for the temperature variation, however) is based on some general arguments concerning two-dimensional hydrodynamics.

0022-2291/84/0400-0083$03.50/0

Additional models for the surface interactions generally appeal to the ubiquity of paramagnetic surface impurities (such as adsorbed O_2),[9–11] but do not reproduce the temperature and field dependences seen in the T_1 experiments.

In addition to the T_1 effects noted above, the surface relaxation of ^{3}He has aroused interest through the context of the anomalous Kapitza resistance. Upon noticing that the Kapitza boundary resistance between ^{3}He and CMN was far below that predicted by theory (and that measured for ^{4}He), Wheatley[12] suggested that there was some sort of ^{3}He magnetic coupling with the substrate. This coupling was to provide the extra channel for heat flow across the interface, which resulted in the low values observed for R_K. These low values are recognized as being quite fortunate from the cryogenic viewpoint, since they permit ^{3}He experiments at temperatures that could otherwise not be attained. Leggett and Vuorio[13] expanded along these lines by constructing a theory in which the ^{3}He quasiparticles were scattered due to magnetic interactions between the ^{3}He spin and paramagnetic surface sites. Others have since extended this framework[14,15] to include additional surface effects as well.[16] A review of the experiments and theory concerned with the R_K problem is given by Harrison.[17]

Nuclear magnetic resonance offers a very clean means to focus on the problems of magnetic interactions between ^{3}He and surfaces. The very short T_1 values measured for ^{3}He in restricted geometries are undoubtedly due to surface interactions of some sort. Recalling that a T_1 value directly characterizes the flow of energy between the ^{3}He spin reservoir and the outside world, it should be apparent that the anomalous R_K effect may represent a closely related measurement. But there are nonmagnetic contributions to the heat flow between ^{3}He liquid and a substrate, so that it is difficult to separate out the various components in an R_K measurement. The T_1 recovery for the ^{3}He spin system, however, depends strictly on the magnetic interactions and is therefore preferable in this regard.

The present work affords an additional handle on the problem of surface relaxation. It was our intention to study the important interface region from both sides. To this end we chose a fluorocarbon substrate so that both the fluorine and ^{3}He properties could be monitored via NMR. Bulk relaxation for similar fluorocarbon insulators had been seen to be quite long, indicating that surface effects were again expected to dominate the fluorine behavior so long as the fluorine spins could somehow sense the surface presence.[18] For this we relied on the diffusive motion for the ^{19}F magnetization that arises through the dipolar interactions of neighbors inducing mutual spin flips. Using typical values for spin diffusion in solids, we estimated this diffusive time constant to be around 20 sec for our 2000-Å-diameter fluorocarbon spheres. Since this was far shorter than

expected bulk T_1 values, any surface effects relevant for ^{3}He relaxation might also be thought to influence the ^{19}F.

The general hope in these experiments was to find features in the ^{3}He behavior that were common with the surface-dominated substrate relaxation. Our work with the fluorocarbon substrate in fact led us to observe an unexpected sort of surface interaction for ^{3}He. We shall describe several experiments that show the existence of a strong nuclear coupling between ^{3}He and the ^{19}F spin species in the substrate. Although the origin of this interaction is as yet indefinite, the interaction itself represents a different means to study various aspects important to ^{3}He relaxation.

2. EXPERIMENTAL

The resonance experiments were all performed using a cryostat cooled by means of a pumped ^{3}He pot with a minimum temperature of 0.35 K. Intermediate temperatures necessary for ^{3}He condensation were attained by pumping the ^{4}He bath down to 1.25 K. Both carbon resistors and ^{19}F susceptibility were used for cell thermometry. The carbon resistors were referenced to a CMN susceptibility calibrated germanium resistor, while the ^{19}F signal was referenced to the 4.2 K bath.

The NMR cells were machined out of epoxy cast with about a 20% fill fraction of #36 Cu wires. The wires, of course, were intended to aid thermal conductivity through the epoxy. One large cell with a 6 cm^3 volume was used during the ^{3}He coverage experiments in which the fluorine T_1 behavior was correlated with ^{3}He adsorption isotherms (see Fig. 8). All other stages in the ^{19}F–^{3}He experiments were performed using cells with 0.2 cm^3 as a typical coil volume. The ^{3}He sample doses could be added to the cells through vacuum-insulated fill lines. These capillaries were equipped with inner and outer heater wires to preclude the plating of ^{3}He as the lines passed through the ^{4}He bath region. After plating a ^{3}He dose onto the substrate surface, we would anneal the sample at approximately 7 K for 2 h to ensure uniform coverage.

The substrate used in these experiments was a saturated fluorocarbon polymer $(CF_2)_x$, marketed by Dupont under the name DLX6000 Microspheres (Dupont Co., Wilmington, Delaware). Figure 1 shows an electron micrograph of these 2000-Å-diameter microspheres. The rather uniform size distribution seen here is typical of the samples we viewed. The microspheres are intended as a plastic additive or lubricant, whereas their redeeming feature for our experiments was merely the presence of the spin-$\frac{1}{2}$ fluorine species. Adsorption isotherms indicated a monolayer ^{3}He dose as being 3.8 STP cm^3 per gram of DLX6000. This was in good agreement with geometrical estimates of the surface area based on electron

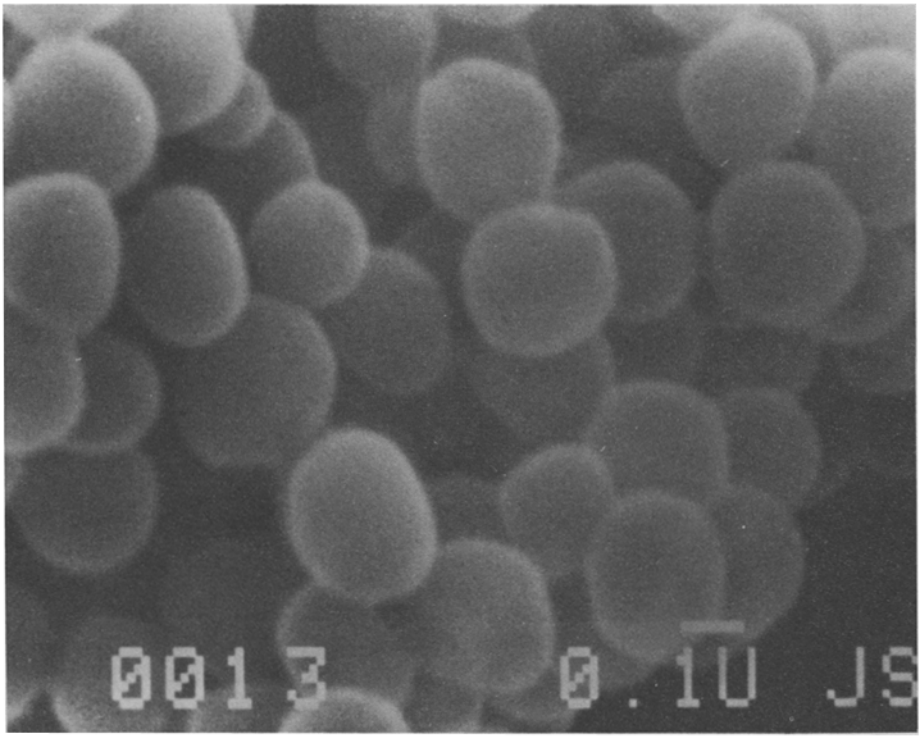

Fig. 1. A scanning electron micrograph of the DLX6000 fluorocarbon particles. The bar in the right corner represents a length of 0.1 μm.

microscope pictures to determine particle size, and Dupont's figures for the bulk density. To increase the effective surface area for our samples, we first compressed the fluorocarbon powder using a machined brass jig and a commercial press. In this manner we were able to attain a 50% fill fraction in the cell volume. After subjecting the powder to approximately 1000 psi, it formed brittle pellets, which could easily be slid into the NMR coil space.

In a previous set of experiments[19,20] we noticed very large differences in the fluorine relaxation times resulting from changes in the substrate O_2 environment. To preclude the O_2 effects it was necessary to clean the sample through repeated N_2 flushings at 100°C. Another means for accomplishing this was merely to subject the sample to a fast thermal cycle. After an initial ^{4}He transfer the NMR cell was heated to approximately 120 K with liquid ^{4}He in the dewar but without gas in the exchange gas can. By then admitting a small quantity of ^{4}He we could cool the sample cell rapidly to 4 K in perhaps 10–20 min. The rapid cooling was thought to favor the plating out

of the O_2 gas (desorbed at 120 K) on the cell walls rather than the substrate surface. The ^{19}F T_1 values resulting from this procedure were characteristic of our cleanest (most thoroughly flushed) samples.

Although the NMR electronics was fairly standard in design, it is worth noting a few details of the pulse methods used for these measurements. The long ^{19}F relaxation times presented concerns that differed somewhat from those one might normally encounter for a short-T_1 species. One such instance involved the measurements of fluorine T_1 and susceptibilities when there was no ^{3}He in the cell (see Fig. 5). The ^{19}F T_1 values were in some cases over 10^4 sec, so that the thermal equilibrium necessary for a susceptibility measurement might require at least a day (even longer with the nonexponential recoveries that were typical). The actual ^{19}F signal, however, was so large that a mere 3° tipping pulse was sufficient to attain reasonable signals. Since 97% of the initial magnetization remained after 20 such pulses, we were easily able to nondestructively monitor the ^{19}F magnetization. Typically, a series of these short sampling pulses was used to monitor a single recovery of the fluorine spins following saturation and thus arrive at a T_1 value. In contrast, relaxation measurements using a 180°–90° sequence would have required many T_1 intervals to determine a T_1 value.

In order to find an accurate value for the equilibrium magnetization M_0, we observed the time evolution of the magnetization for values both greater and less than the actual equilibrium M_0. As seen in Fig. 2, with the magnetization less than the equilibrium M_0, $M(t)$ would increase with time (region A). The process could be considerably hurried by ramping up the magnet current and allowing the sample to spend time (regions B and D) in a high H_0 field. The $M(t)$ would then increase faster than in the lower field and even surpass the low-field equilibrium M_0. Subsequent small-angle

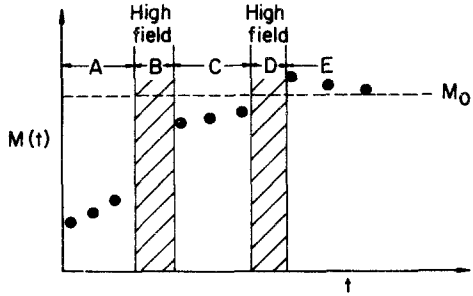

Fig. 2. Allowing the ^{19}F spins to spend time in a high magnetic field (B and D) results in an increasing (A and C) or decreasing (E) magnetization versus time. This sets unambiguous limits on the equilibrium magnetization M_0.

measurements would then reveal whether the measured $M(t)$ was either above [$M(t)$ decreasing, as in region E] or below [$M(t)$ increasing, as in region C] the equilibrium M_0. In this manner it was possible to set unambiguous limits on M_0 without worrying about spurious effects arising from nonexponential recoveries.

The use of short sampling pulses generally allowed us to avoid the tedium of fine tuning the pulse lengths and phases. On the rare occasions when accurate ^{19}F pulse lengths were required (such as during the ^{19}F–^{3}He inversion sequences, Fig. 3), we used the ^{3}He signal for tuning rather than dealing with the long T_1 of the ^{19}F species. A high-precision NMR field lock in the magnet allowed us to first adjust the electronics by observing the ^{3}He signal at some frequency f_0. The field could then be accurately altered to bring the ^{19}F resonance to this already tuned frequency.

3. EXPERIMENTAL RESULTS

Much attention in the field has been focused on what role magnetic impurities might occupy in the processes governing ^{3}He behavior in restricted geometries. Because the relaxation effects from electronic impurities were generally thought to be more important than nuclear spins, there has been no prior work dealing directly with the possibility of ^{3}He interactions with any nuclear substrate species. The data we present will show that these interactions may be a major factor influencing the behavior of ^{3}He close to a substrate containing nuclear spins. Since most popular substrates do at least contain some isotope with a nonvanishing moment, the scope of such effects may be very wide indeed. From a slightly different perspective, the presence of such an interaction will be seen to provide a very useful surface probe. Some later experiments began to use this probe as a means to help detail additional features relevant for ^{3}He relaxation.

3.1. Inversion Experiments

Figure 3 depicts the unusual NMR behavior that underlies much of the present work.[21] The experiment involved monitoring both the ^{19}F and ^{3}He magnetization following a near 180° pulse on just the ^{19}F spins. The data were collected at 1 K and 1.1 kG with roughly one monolayer of ^{3}He adsorbed on the surface. Figure 3a considered alone shows the time evolution of the ^{19}F magnetization in a typical NMR experiment for which the system starts out in thermal equilibrium (during times $t<0$) with $M_z = M_0$. The pulse applied at $t=0$ inverts the magnetization so that it points along the negative z axis (antiparallel to the applied H_0 field). Notice that for subsequent times on the order of 40 sec, the ^{19}F magnetization recovers

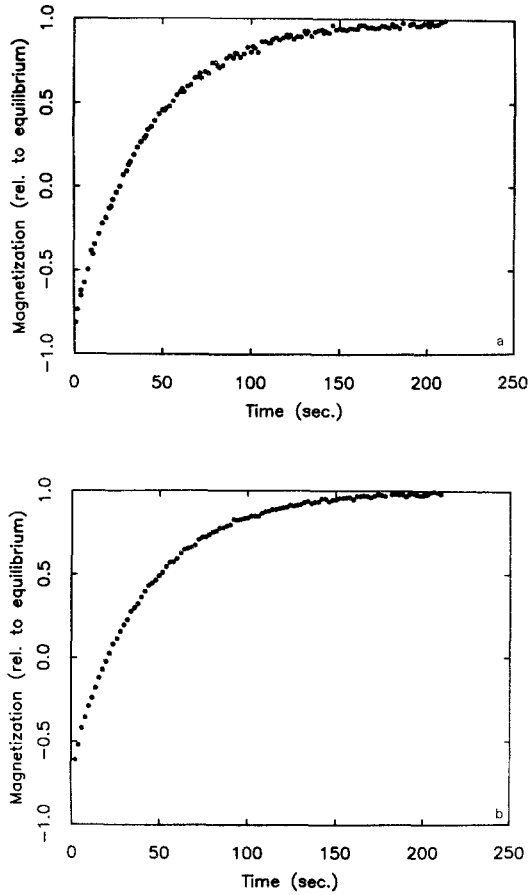

Fig. 3. (a) Magnetization of ^{19}F versus time following a 180° pulse at the ^{19}F resonant frequency. The rf frequency was 4.45 MHz and the temperature was 1 K. The fluorine magnetization first inverts and then recovers toward the thermal equilibrium value with a time constant of about 40 sec. (b) Magnetization of ^{3}He versus time under the same conditions of field and temperature as (a). The ^{3}He resonant frequency was 3.6 MHz. The applied rf pulse was at the ^{19}F resonant frequency, the same initial pulse used in (a). The coupling between the ^{19}F and ^{3}He causes the ^{3}He spins to invert and recover with much the same time constant as the ^{19}F. (c) Recovery of ^{3}He magnetization following a 180° pulse applied at the ^{3}He resonant frequency. This is the conventional experiment for measuring the quantity T_1. In this case the ^{3}He spins recover with a 40-msec time constant. The recovery is three orders of magnitude more rapid than that observed for either ^{3}He or ^{19}F when an rf pulse is used to invert the ^{19}F spins initially.

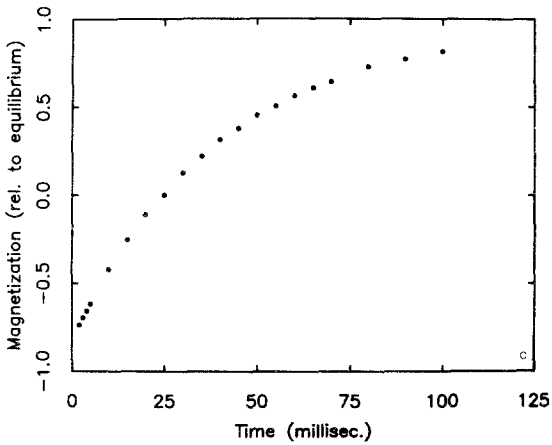

Fig. 3. Continued.

back to thermal equilibrium. The time constant associated with the recovery seen on such curves is, of course, the thermal relaxation time T_1.

The surprise arises when we view the behavior of the adsorbed ^{3}He monolayer simultaneously with that for the ^{19}F. Although the 180° pulse applied at $t=0$ was at the resonant frequency of the ^{19}F spins, the ^{3}He magnetization shows a marked response to it. Figure 3b displays how in such an instance the time evolution of the ^{3}He magnetization closely mimics that of the ^{19}F. Following the 180° pulse on the ^{19}F spins, the ^{3}He magnetization first inverts and then recovers with the same 40-sec time constant seen in Fig. 3a for the ^{19}F system. This is in sharp contrast to the 40-msec T_1 measured for ^{3}He in the conventional manner. The 40-msec time may be derived from the plot appearing in Fig. 3c. In this instance, the thermal equilibrium of the ^{3}He is disrupted through a pulse applied at the ^{3}He frequency. The recovery of the ^{3}He magnetization is then seen to occur with the short 40-msec T_1 instead of the 40-sec recovery in Fig. 3b. At higher frequencies the time constants measured by these two methods increase considerably, but maintain the marked contrast seen in Fig. 3. With $H_0=4$ kG, for example, the ^{19}F–^{3}He recoveries in response to a resonant fluorine pulse (Figs. 3a and 3b) reach 10^3 sec, while the ^{3}He T_1 of Fig. 3c increases to 200 msec.

A somewhat related form of the effect seen in Fig. 3 could be observed by merely saturating either of the two spin species. As one might suspect from Fig. 3, setting the fluorine magnetization equal to zero (by applying a 90° rather than 180° pulse) would result in a zeroed magnetization for ^{3}He as well. But the reverse effect was also observed when the ^{3}He signal was saturated. For example, with $H_0=4$ kG a few hundred 90° pulses applied at the ^{3}He frequency with a rate of several per second (recall that

the measured T_1 under such conditions was 200 msec) would result in a fluorine magnetization roughly half that observed in equilibrium. Eddy current heating was not responsible for the increase in ^{19}F temperature, as no such effect was observed if the pulses were not at the ^{3}He frequency. This merely reflected the fact that the spin temperatures of the ^{19}F and ^{3}He were in close communication regardless of which magnetization was being directly altered by the applied rf. Once the ^{19}F magnetization had been so degraded, however, it required several T_1 intervals (several thousand seconds) to recover after the ^{3}He pulses ceased. The ^{3}He, of course, displayed a diminished signal for the same length of time since its spin temperature was pinned to that of the fluorine.

This sort of behavior for the ^{3}He was the signature of a two-bath effect, only in this instance the data had clearly identified which two reservoirs were involved. The contact between the two spin reservoirs would therefore create a marked difference in the ^{3}He behavior following a short, as opposed to long, interval of saturation. To be explicit, any mild irradiation at the ^{3}He frequency (such as that from just a few pulses) had little effect on the ^{19}F reservoir. But prolonged heating of the ^{3}He allowed heat to trickle into the ^{19}F reservoir and ultimately cause a diminished ^{19}F magnetization. This degraded ^{19}F signal would then persist for several times T_1 once the heating had ended and, in addition, drag the ^{3}He magnetization down for the same interval. This type of two-bath behavior has been previously noted in ^{3}He experiments. Goto,[22] for example, observed these same differences between the long and short saturation pulses for ^{3}He adsorbed on Vycor. He attributed this to a two-bath effect arising from a contact between the ^{3}He spin and tunneling motion reservoirs. It is possible, however, that the 5% abundant ^{29}Si isotope in the Vycor substrate could have been a second reservoir in contact with the ^{3}He.

The two-bath contact that could degrade our ^{3}He signals for times typical of the ^{19}F T_1 value also served as a means to enhance these ^{3}He signals for like intervals. Starting with a 13-MHz ($H_0 \sim 4$ kG) ^{3}He resonance, the field was ramped up to 10 kG, where the spin systems were allowed to equilibrate for several hours. At this field, the equilibrium magnetization for both the ^{19}F and ^{3}He was, of course, 2.5 times that for the 4-kG field. Upon returning the field to 4 kG and monitoring the ^{3}He signal, we observed this enhanced magnetization to persist for times again typical of a ^{19}F T_1. Without the contact to the ^{19}F reservoir, however, this enhanced ^{3}He magnetization would have vanished after only a few ^{3}He T_1 intervals (i.e., after just a few seconds). It should be apparent that any method of enhancing the substrate magnetization could offer a means to achieve enhanced ^{3}He signals as well. One such approach has already been attempted on this substrate, and has met with encouraging results.[23]

The two-bath picture offers one simple framework to view the processes underlying the curves displayed in Fig. 3. It has already become apparent that the strong ^{3}He–^{19}F link allows the two systems to rapidly equilibrate. A further question still arises concerning the time required for this equilibrium to occur. To address this it need only be recalled that the T_1 measured for ^{3}He directly was only 40 msec. The natural interpretation might therefore be that this 40 msec was in fact just a measure of this equilibrium time required for the small ^{3}He reservoir to thermalize with the ^{19}F spins.

To test this picture, we performed the experiment summarized in Figure 4. The ^{19}F population was first inverted with a 180° pulse at the fluorine frequency, leading in addition to a ^{3}He inversion as was described earlier. The solid line in Fig. 4 represents this same sort of slow ^{3}He recovery we saw in Fig. 3b. In this instance, we sought to drive the ^{3}He magnetization away from its equilibrium with the ^{19}F reservoir (i.e. away from the solid curve). For this we applied pulses at the ^{3}He resonant frequency to directly invert the ^{3}He spins. The intention here was to measure the time required for the surface interactions to pull the ^{3}He magnetization back into equilibrium with the ^{19}F reservoir (i.e., back to the slow recovery curve). The dashed lines in Fig. 4 clarify the sort of ^{3}He response seen following the 180° pulses applied at the ^{3}He resonant frequency. We observe that after any 180° pulse at the ^{3}He frequency, the ^{3}He spins quickly return to

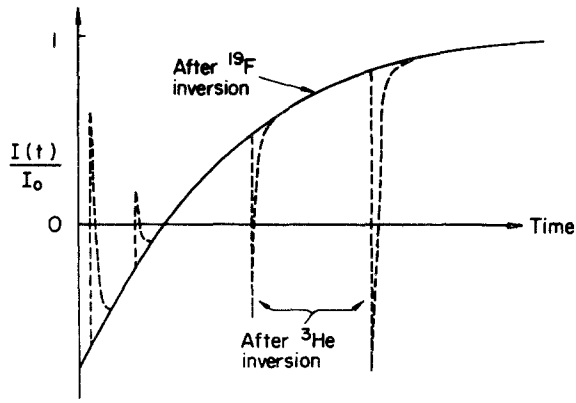

Fig. 4. The ^{3}He magnetization versus time. This is another variation of the experiment shown in Fig. 3b. A 180° rf pulse is applied initially at the ^{19}F frequency. The ^{3}He spins are rapidly inverted by the magnetic coupling at the interface with the ^{19}F. If 180° pulses are applied at the ^{3}He frequency while the ^{19}F is recovering to equilibrium, the ^{3}He reverses its direction of magnetization but then recovers to the polarization apparently determined by the ^{19}F substrate. The rapid recovery, illustrated with a dashed curve, has a 40-msec time constant.

equilibrium with the ^{19}F reservoir. This is evident from the short interval required for the dashed and solid lines to merge. This interval was measured with standard T_1-type pulse sequences. The time constant for these dashed curves was thus found to be roughly 40 msec, in agreement with the previous measurements of ^{3}He T_1 values. In this context, what was pictured as a ^{3}He T_1 measurement could be represented as one of the dashed lines in Fig. 4 recorded at a sufficiently long time on the solid curve so that $S(t)/S(0) \approx 1$ (i.e., with the ^{3}He and ^{19}F spin reservoirs in thermal equilibrium with the lattice). The interpretation suggested by this is merely that the 40-msec interval in both instances represents the time required for the ^{3}He–^{19}F equilibration. The direct measurement of the ^{3}He T_1 would therefore not be a good indication of contact between the ^{3}He and a lattice reservoir. The processes being probed are, in fact, quite different from those normally thought to govern a T_1 measurement. Note, in addition, that the processes relevant for the ^{3}He T_1 measurement do little to alter the net number pf (^{3}He+^{19}F) spins aligned with the field. Since the solid curve in Fig. 4 slowly returns to thermal equilibrium with the lattice reservoir, it is evident that there must also be some lattice link that does change this net number of aligned spins. Section 3.2 will deal more fully with this aspect.

It is noteworthy that the ^{19}F–^{3}He coupling thus far appears active at lower temperatures. Again working with the DLX6000 substrate, Hammel *et al.*[24] and Chapellier[25] have observed ^{19}F–^{3}He communication extending into the millikelvin temperature range. Some initial suggestions[23] for a possible coupling mechanism would have predicted the ^{19}F–^{3}He link to virtually vanish in this regime. The fact that the communication remains means that these interactions of ^{3}He with nuclear spins in a wall may be important for those experiments performed even at the lowest temperatures.

The sort of coupling evident through the ^{3}He inversion experiments showed no sign of being present in the fluorocarbon bulk. Working again at 1 K and 4 kG, we checked for, but did not detect, communication between the 1% abundant ^{13}C and ^{19}F spins. The ^{19}F/^{13}C number ratio was comparable to that in the ^{3}He version of this experiment. While monitoring the ^{13}C signal, however, we observed no changes when the ^{19}F spins were inverted through application of a 180° pulse. Curiously, the ^{13}C T_1 was only a few seconds (even with the ^{19}F T_1 on the order of 10^3 sec), so there was no means to check for surface communication between the ^{13}C and ^{3}He. That is, since the ^{13}C diffusion time was larger than the T_1, any surface effect would never be sensed by the bulk ^{13}C. Still, the bulk properties were insufficient to produce any trace of ^{13}C–^{19}F coupling comparable to that observed for the ^{19}F–^{3}He systems at the surface. Although we cannot unambiguously identify the reservoirs and their coupling responsible for the ^{3}He–^{19}F communication, it is nonetheless quite evident that some surface property must play an essential role.

3.2. Coverage Experiments

The inversion experiments described in Section 3.1 demonstrated that the magnetization of the substrate ^{19}F spins could be transferred to the surface ^{3}He spins. It might not be too surprising, then, if fluorine recovery times were somehow altered by the presence of this strongly coupled reservoir. Figure 5 reinforces this notion by displaying the temperature dependence for the ^{19}F T_1 values in the presence and absence of adsorbed ^{3}He. With the cell empty of any ^{3}He, the ^{19}F T_1 values are more than an order of magnitude larger than observed for the cell when ^{3}He fills the pores. Figure 5 is itself a clear sign that some sort of communication occurs between the ^{3}He and substrate nuclei. Thermal contact with the substrate did not in this instance introduce any ambiguities, as the ^{19}F susceptibility agreed well with the resistance thermometer for both runs, and the ^{3}He susceptibility matched that of the published bulk values[26]. In addition, the long ^{19}F T_1 values were unaltered when ^{4}He was added to the cell instead of ^{3}He. Apparently, the ^{3}He spin was the ingredient necessary to produce the short ^{19}F relaxation times. The qualitative difference between the two curves in Fig. 5 brings to mind the T_1 curves for ^{3}He alone seen in restricted geometry experiments.[6,7] For without ^{3}He in the cell the ^{19}F T_1 appears to continue increasing as the temperature is lowered. But the T_1 measured for the cell filled with ^{3}He shows the same flattening out at the lower

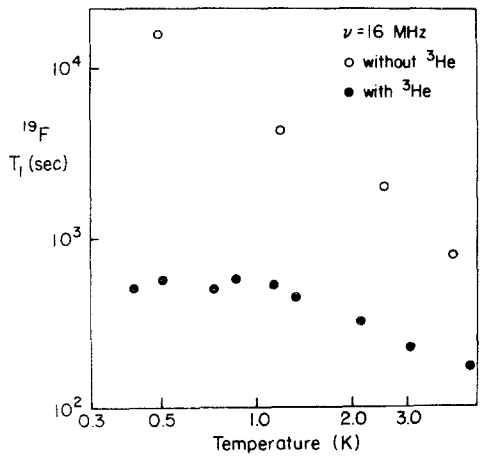

Fig. 5. Time constants T_1 of ^{19}F with and without ^{3}He adsorbed on the surface. The ^{3}He plating results in an order of magnitude change in the ^{19}F time constant and a qualitative difference in the temperature behavior.

temperatures as was seen for the ^{3}He itself. This strongly suggests that the ^{3}He relaxation channels have been opened to the ^{19}F through the surface communication, hence resulting in a ^{19}F T_1 behavior that mimics that of ^{3}He. Since these previous studies have seen such ^{3}He T_1 values to start decreasing again at still lower temperatures, it would be interesting to monitor the ^{19}F T_1 behavior throughout these same regions to determine whether the ^{19}F T_1 behavior does likewise.

The large T_1 differences seen in Fig. 5 were measured for the limits where a cell was either completely empty or full of ^{3}He. It seemed that further details concerning the ^{19}F–^{3}He interaction might be obtained by varying the ^{3}He surface coverage more slowly between these two extremes. Figure 6 summarizes the ^{19}F T_1 values obtained at 1 K and 4 kG as small doses of ^{3}He were successively added to the cell. The curve reveals there to be an unexpected amount of structure at these submonolayer doses. For very low coverages the ^{19}F relaxation rate appears rather insensitive to the presence of ^{3}He on the surface. After some critical coverage, however, further ^{3}He additions result in a rapid increase in $1/T_1$ followed by a very sharp minimum and a broad maximum. The slowly decreasing tail evident further out on the curve continues for at least twice the ^{3}He dose required for the preceding broad maximum. The "intrinsic" relaxation rate efficiency available to the ^{19}F spins is indicated by the zero-coverage point at 1.8×10^{-4} sec^{-1}.

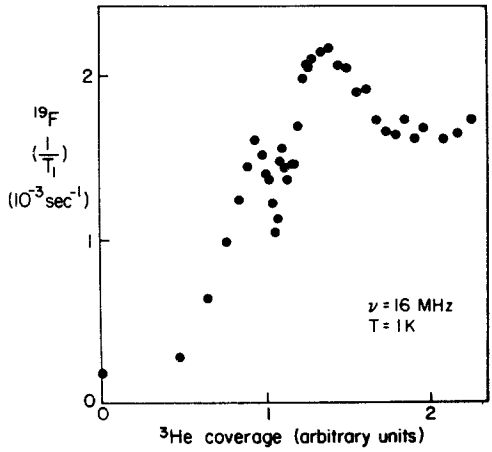

Fig. 6. Changes in the ^{19}F relaxation rate with a varying amount of ^{3}He on the substrate. The experiment was performed at 1 K with a ^{19}F resonant frequency of 16 MHz.

The experiments in this and the preceding section provide a means to model the general pathway required for the ^{19}F relaxation. Figures 5 and 6 indicate that once the ^{19}F spins have been saturated, the primary means for refreshing the magnetization arises from the ^{3}He adsorbed on the surface. The T_1 measured for the ^{19}F will therefore be governed by the times required in the series pathway that brings magnetization from the surface to the bulk. This pathway includes both the ^{3}He–^{19}F surface communication and the ^{19}F spin diffusion within the fluorocarbon bead itself. The measured T_1 values, however, are sufficiently long that such diffusion has time to maintain a fairly uniform bulk magnetization throughout the recovery: the bottleneck for the ^{19}F relaxation must therefore be associated with what happens on the surface.

The inversion experiments (Section 3.1) have indicated the dominant feature in the ^{19}F–^{3}He communication to be the easy transfor of magnetization between the two spin systems. But this single process cannot significantly alter the total ($^{3}He+^{19}F$ together) fraction of spins aligned with the H_0 field and thus cannot thermalize the spin baths with the lattice reservoir. There must instead be mechanisms that directly alter only the ^{19}F or ^{3}He magnetization alone. In the latter case, the ^{19}F relaxation would be a two-step process requiring the initial exchange of magnetization with ^{3}He spins and the subsequent relaxation within the ^{3}He bath. We shall term the second step "direct": by this we mean a process for which the ^{3}He magnetization changes without altering that of the ^{19}F. A two-step fluorine T_1 so determined could be expressed as

$$T_1^{\text{meas}} = (T_1^{IS} + T_1^I)(N_S/N_I) \tag{1}$$

with $I = {}^{3}He$ spins and $S = {}^{19}F$ spins. Here the T_1^{IS} represents the mixing time of the ^{3}He with the ^{19}F bath and T_1^I is the direct relaxation time for the ^{3}He spins alone. The N_S/N_I factor arises since each of the N_I ^{3}He spins on the surface must bear the burden of relaxing N_S ^{19}F spins in order that the latter equilibrate. Adsorption experiments set this ratio to be roughly 300 for the (0.8) ^{3}He coverage (Fig. 6) corresponding to a ^{19}F T_1 of 10^3 sec, so that

$$T_1^{IS} + T_1^I \approx 10^3/300 \quad \text{sec} \tag{2}$$

or

$$T_1^I \approx \text{few seconds} \tag{3}$$

since T_1^{IS} is only around 200 msec (see Figs. 3c and 4, where the 1.1 kG measurement of T_1^{IS} was 40 msec). We may thus identify Eq. (3) as defining the time scale for the direct relaxation of ^{3}He alone. The same time scale would hold if we assumed that the ^{19}F relaxed directly through its interaction with ^{3}He [i.e., a one-step surface relaxation process as opposed to Eq. (1)].

Figure 7 illustrates the reservoirs and time constants included in the relaxation processes. The most efficient relaxation for the bulk ^{19}F is pictured as occurring through the intermediate surface reservoirs. The two-step process of Eq. (1), for example, follows a pathway from the ^{19}F bulk through the ^{19}F and ^{3}He surface spin reservoirs, and finally to the thermal lattice. The availability of this pathway makes it evident that Eq. (3) at least puts a lower bound on T_1^I. The strong ^{19}F–^{3}He contact (characterized by $T_1^{IS} \approx$ 200 msec) ensures that a ^{3}He T_1^I shorter than a few seconds would have to result in a ^{19}F relaxation time shorter than measured (i.e., shorter than 1000 sec). If some direct ^{19}F relaxation (noted in Fig. 7 with a T_1^S time constant) acts in parallel with the two-step process of Eq. (1), the T_1^{meas} for the bulk ^{19}F signal may be seen as placing a lower bound on both this T_1^S and the T_1^I of the ^{3}He as well. The T_1^{meas} for the bulk ^{19}F signal may in this sense be seen as a measure of the ^{3}He relaxation processes. We suspected this earlier from the similar temperature dependences of the ^{19}F and ^{3}He relaxation times, and Fig. 7 provides a means to consider why such similarities might arise.

This general model for the surface relaxation suggests that we may view the ^{19}F behavior as a probe of the ^{3}He T_1^I. The initial flat region (followed by the knee) could conceivably arise from several effects. One obvious possibility is that the $1/T_1^I$ process is a cooperative phenomenon for which the ^{3}He atoms must actually see their neighbors. Low doses would then have little effect on the relaxation efficiency, since the spins would be too far apart on the surface for this to occur. But the same insensitivity could result if the ^{3}He surface mobility is an important factor governing the $1/T_1^I$ efficiency. The flat region might then arise if the initial doses were

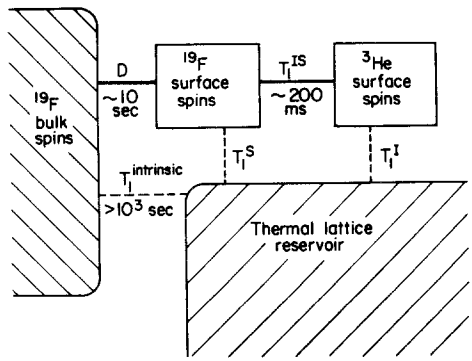

Fig. 7. The various spin and thermal reservoirs of the system communicate with different time constants.

more tightly bound to the surface than later ones. A surface mobility influence would probably also be seen at monolayer completion in addition, since closely packing ^{3}He atoms would change the character of the motion from the lower coverages. A greater mobility for ^{3}He layers beyond the first could then affect the ^{19}F T_1^{meas} as well, although the weaker interaction of these distant layers with the surface would have to impede any relaxation efficiency. These considerations made it necessary to make a better determination of the ^{3}He monolayer dosage.

Since the earlier sample contained a surface area too small for calibration purposes, a 6-cm^3 cell was constructed with an anticipated sample surface close to 100 m^2. Figure 8 displays the ^{19}F relaxation data for the new cell, with the horizontal axis measured in STP cm^3 of ^{3}He per gram of DLX6000 sample in the cell. These data were gathered at 1 K and a 6-MHz ^{19}F resonant frequency. Note that the same general features that were pointed out for Fig. 6 are again evident here. The minimum at 3.8 cm^3/g appears in Fig. 8 to fall only to a level comparable to the rates seen in the long tail (i.e., past 5 cm^3/g coverages). It seems likely that the differences between the two experiments are related to the frequency: with the higher ^{19}F resonant frequency (16 MHz for Fig. 6) the dip is seen to extend far beneath the high-coverage tail.

A nitrogen BET[27] performed on this sample resulted in an N_2 monolayer of 2.7 cm^3/g. Accounting for the differences in surface areas,

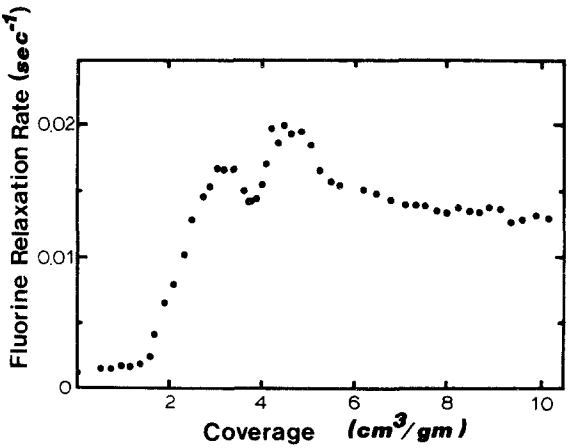

Fig. 8. The relaxation rate of ^{19}F at 1 K with a resonant frequency of 6 MHz. The same basic structure that was seen with ^{3}He coverage changes at 16 MHz is also seen in this lower magnetic field. Adsorption experiments indicated that the coverage required for one monolayer of ^{3}He was 3.8 STP cm^3 per gram of DLX6000.

this results in a $2.7 \cdot 13.6/10 = 3.6\,\mathrm{cm}^3/\mathrm{g}$ dose for the ^{3}He monolayer. It seems reasonable to then associate the $1/T_1$ dip of Fig. 8 with some aspect of monolayer completion for the ^{3}He. The subsequent broad maximum (followed by the long tail) then corresponds to ^{3}He additions in the second layer. Any ^{19}F T_1 sensitivity to a second ^{3}He layer is indeed noteworthy since it signals the presence of efficient relaxation for these ^{3}He atoms more distant from the interface. Ordinarily, the heightened surface relaxation for ^{3}He is associated with the local properties of the surface, such as imbedded paramagnetic impurities: the ^{19}F data, however, now point to the possibility that the details of the solid layers may themselves represent important ^{3}He relaxation channels.

The region of the $1/T_1$ curve associated with monolayer completion shows an interesting temperature dependence. Figure 9 highlights the

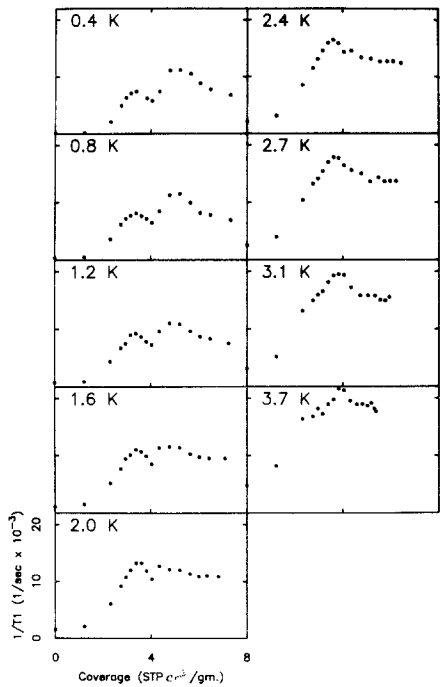

Fig. 9. Measurements of ^{19}F relaxation rate with ^{3}He coverage at various temperatures. The measurements were made with a ^{19}F resonant frequency of 10 MHz. The sharp minimum in the relaxation rate seen at low temperatures with a coverage of 4 STP cm^3 per gram of DLX6000 disappears as the temperature is raised.

changes seen in these features between the temperatures of 0.4 and 3.6 K. Talbe I in the Appendix lists the 10-MHz data of Fig. 9. As the temperature is increased from curve a through i we see a general smearing of any monolayer-type features. The sharp minimum that is clearly evident in curve a is all but gone by the 2.4 K curve f. Notice, in addition, that the broad maximum and the long tail that follows it rise in height considerably as the temperature is increased. Since these temperatures are well below that at which we could expect significant ^{3}He description, we must consider other possible explanations for Fig. 9.

The changes in the curve might suggest that the ^{19}F $1/T_1$ features arise in part from the ^{3}He surface geometry. Thermal excitations prompted by the increased temperature could be expected to compete with any tendency to form a well-defined surface structure near monolayer coverages. If the time scale of the ^{3}He motion on the surface influences either the direct ^{3}He relaxation or the ^{3}He–^{19}F communication, such changes in the surface would then show up in the measured ^{19}F relaxation rates. It might be interesting to correlate these ^{19}F $1/T_1$ curves with additional linewidth studies on the ^{3}He or heat capacity measurements in order to further probe what is occurring in this temperature regime and clarify the ^{3}He role in ^{19}F relaxation.

We have seen how features in the ^{19}F data occurring at ^{3}He monolayer completion imply that the details of the surface conditions play an important role in the surface relaxation process. This is further reinforced by some trials that involved first preplating the DLX6000 surface with a small ^{4}He dose. Figure 10 shows some ^{19}F relaxation rates measured for rather low ^{3}He coverages at the same field and temperature as Fig. 8. The open circles merely represent a finer grid of points than appear in Fig. 8, so as to emphasize these low-coverage features. We see that the so-called flat region does in fact display a slight nonzero slope and looks fairly linear out to 1.6 cm^3/g. At this latter coverage the rise in ^{19}F relaxation rates produces a sharp knee in the curve, as we noted earlier.

To help interpret the cause of this behavior we preplated the surface with a 1.6 cm^3/g ^{4}He dose. This quantity roughly matched that required for the ^{3}He to produce the knee in the open circle data. The closed circles in Fig. 10 denote the relaxation rates obtained with the surface so prepared. Note that the horizontal axis excludes the initial ^{4}He dose and only indicates the amount of ^{3}He in the cell. If the knee were due to a relaxation channel that relied on ^{3}He–^{3}He spin interactions, the preplating could only have reduced the effect of ^{3}He on the surface: in this case ^{3}He coverages of at least 1.6 cm^3/g would still have been required to ensure efficient ^{19}F relaxation. But we see in Fig. 10 that the closed circle rates rise above those for the plain surface (open circles) at comparable ^{3}He doses. The modicum of

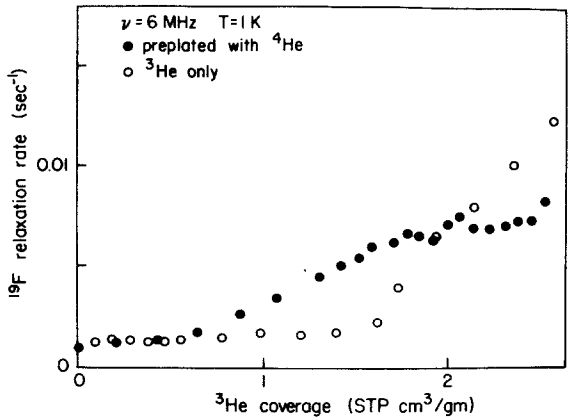

Fig. 10. With the scale expanded from that shown in Fig. 8, we see the effects of ^{4}He preplating for very low ^{3}He doses. The ^{4}He preplated surface (shown by solid circles) actually result in some ^{19}F relaxation rates that are larger than those for the surface without ^{4}He. In this figure the horizontal axis corresponds only to the amount of ^{3}He in the cell.

^{4}He must therefore in some sense aid rather than hinder the ^{3}He in relaxing the ^{19}F nuclei. Trials run with only ^{4}He doses, however, produced no discernible changes in the ^{19}F relaxation rates. This puzzle may be clarified by plotting the data in a somewhat different manner.

The two sets of data for still higher coverages are compared in Fig. 11, where the horizontal axis now indicates the total quantity of ^{3}He + ^{4}He in the cell. The striking aspect of these curves is that the general features are so much alike. We see peaks in both curves at the 5 cm^3/g coverage, and the dip at 3.8 cm^3/g for the pure ^{3}He run appears as a flat region in the ^{3}He + ^{4}He data. The ^{4}He dose included in this second run clearly does not offset the curve from data compiled for ^{3}He alone. Instead, the low ^{4}He dose appears to serve the same function as the comparable amount of ^{3}He in the upper curve, although the rates for pure ^{3}He are somewhat greater than those for the mixture. Still larger amounts of ^{4}He (past 7.4 cm^3/g coverages) are seen to further impede the ^{19}F surface relaxation, for we see that the data (noted with open circles for these later ^{4}He additions) decrease to almost the initial clean surface rate by the time the ^{4}He dose approaches a full monolayer. This clearly shows that ^{4}He itself cannot contribute directly to the ^{19}F surface relaxation. In addition, the ^{19}F–^{3}He interaction must be very short range, since the single ^{4}He layer (which displaces the ^{3}He) all but eliminates the enhanced ^{19}F relaxation induced by the ^{3}He.

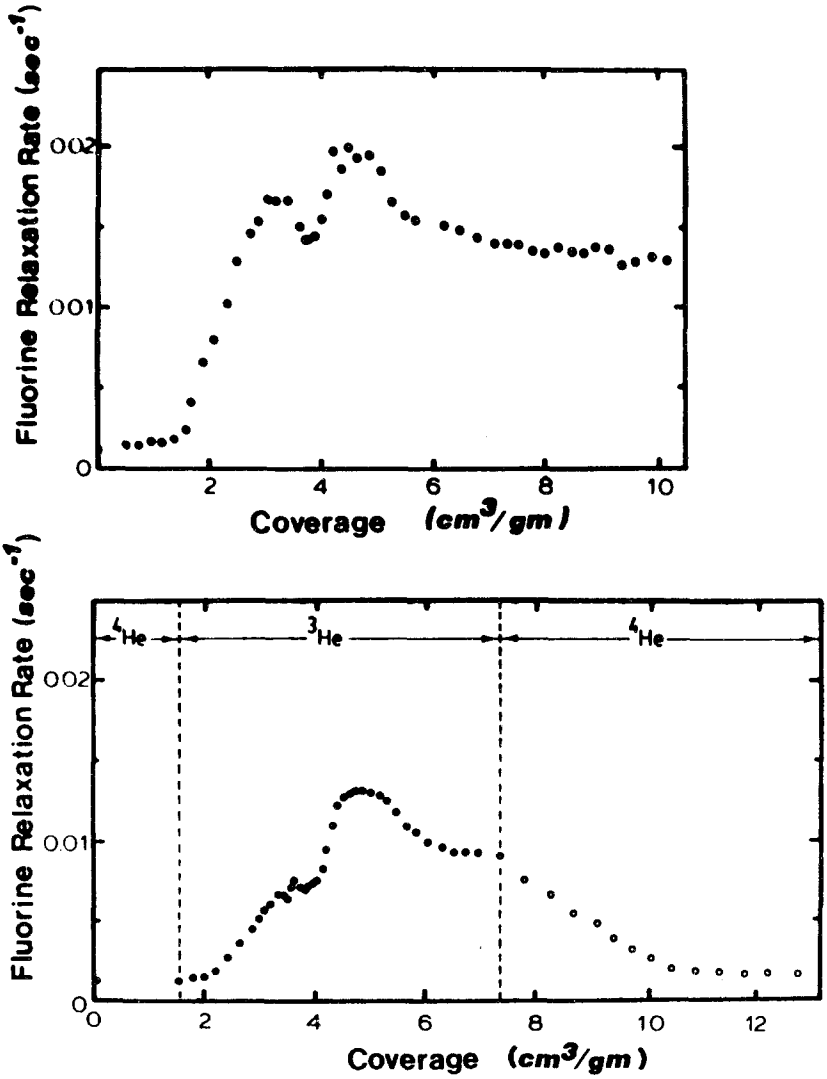

Fig. 11. Comparison of ^{19}F relaxation rate with helium coverage with pure ^{3}He (upper curve) and with initial plating with ^{4}He. The upper curve is the same as Fig. 8. The lower curve shows that with a submonolayer coverage of ^{4}He, the same qualitative features are seen in the relaxation rate with helium coverages near 4 STP cm^3 per gram of DLX6000. Eventually, when enough ^{4}He is added to completely cover the surface, shown for coverages between 7.5 and 10 cm^3 per gram, the relaxation rates drops to nearly the value measured for the bare surface.

But the alignment of the two curves says that the low ^{3}He and ^{4}He doses appear to have similar functions. The role for the initial 1.6 cm^3/g dose must therefore be an inert one for both the ^{3}He and ^{4}He. That is, the first 1.6 cm^3/g merely fills in some surface sites that are unimportant in the ^{19}F relaxation process. It seems likely that the feature that distinguishes these sites is their greater binding energy. This binding energy first ensures that the initial doses occupy these sites preferentially and in addition leads to the reduced relaxation efficiency for any ^{3}He thus bound. The ^{3}He filling such sites might be less mobile than later doses and for this reason contribute less to the ^{19}F relaxation. It is in this sense that the data of Fig. 11 again suggest a possible role for ^{3}He surface motion in the relaxation processes these experiments probe.

A somewhat similar explanation for the effect seen in Fig. 11 is merely that the ^{3}He motion is involved in the relaxation in a manner that becomes more efficient at higher coverages. Relaxation theory language would express this by saying that the T_1^I relaxation is most efficient when the time scale of the motion (which modulates the interactions with the ^{19}F) matches the Larmor frequency for the ^{3}He. In such an instance, nothing distinguishes some fraction of the surface sites, but rather a certain degree of surface crowding is necessary for efficient ^{3}He relaxation. Initial ^{4}He doses would merely need to behave as the ^{3}He in their ability to impede the motion of the subsequent ^{3}He doses. The lower rates for the ^{3}He+^{4}He run in Fig. 11 then arise because of the lower density of ^{3}He on the surface, even though the individual ^{3}He atoms provide efficient relaxation.

We have seen that the communication between the ^{3}He and ^{19}F spin systems accounts for the dominant ^{19}F relaxation mechanism. Variations in the ^{19}F relaxation rate may in fact be interpreted as stemming from changes in the relaxation of the adsorbed ^{3}He. A similar assertion, however, cannot be made for the mechanism of bulk ^{3}He relaxation. Previous experiments[19,20] dealing with the effects of oxygen addition revealed that the ^{19}F rates could be markedly altered without showing any changes in the ^{3}He relaxation. The conclusion from this must be that the bulk ^{3}He does not depend on the substrate spin relaxation as a thermalizing source of magnetization. It will soon be apparent that the ^{19}F magnetization, in addition to its T_1, is not an important factor for bulk ^{3}He relaxation.

We have seen that the approach that relies on the ^{19}F data to study the ^{3}He is useful in another sense. The time constants we extract from a ^{19}F T_1 contain information about the ^{3}He relaxation process that is not immediately accessible through experiments on the ^{3}He alone. In addition, the general ^{19}F features noted by varying the ^{3}He coverage have provided hints as to what aspect of the surface is important for ^{3}He relaxation. For instance, the experiments with a monolayer of ^{4}He show that the range of

the ^{19}F–^{3}He interaction is very short. More information of this sort will turn up in the next section, where we again use the ^{19}F–^{3}He link as a surface probe.

3.3. Saturation Experiments

The rather dramatic influence that a substrate spin reservoir may have on the behavior of adsorbed ^{3}He has already been shown through the preceding experiments. One question raised by this pertains to the extent to which this particular surface interaction affects bulk ^{3}He properties. In particular, we wished to learn just how far the influence of ^{19}F–^{3}He magnetization exchange at the interface might penetrate into a bulk ^{3}He sample. The experiment for doing this merely required that we monitor the bulk ^{3}He signal while the substrate ^{19}F magnetization was altered. Although similar in practice to the inversion experiments (Section 3.1), the presence here of bulk ^{3}He made the situation quite different.

Our earlier inversion experiments were performed with a mere film of ^{3}He. At that time we observed that substrate saturation ($M = 0$ for the ^{19}F spins) also resulted in saturation for the adsorbed ^{3}He layer. In an instance where bulk ^{3}He fills the pores it might therefore be reasonable to infer that substrate saturation would still diminish the magnetization of ^{3}He near the surface. Any observation of a smaller ^{3}He signal would confirm the supposition that the ^{3}He spins near the surface had been saturated in response to the substrate treatment.

Working at 1 K and 4 kG, we did in fact observe such an effect on the bulk ^{3}He. Since the ^{19}F T_1 was still 600 sec with the cell full of ^{3}He, it was very easy to maintain ^{19}F saturation by merely applying resonant rf pulses every 10 sec. In between these pulses, the ^{3}He signal could easily be monitored. This scheme ensured that no spurious effects could arise from cross-talk between the two spectrometers. When the frequency of the saturating pulses for the ^{19}F was shifted off resonance, the ^{3}He signal returned to its full size, thus eliminating the possibility that rf heating was the cause of the effects seen. The decrease in the ^{3}He signal under such conditions amounted to 35% of that observed with the system in thermal equilibrium. With the setup used for these measurements it was not convenient to record the time constant with which the ^{3}He signal decayed to 0.65 its original size. In the inversion experiments (Section 3.1) we observed that the ^{3}He–^{19}F communication occurred at this frequency on a time scale of approximately 200 msec. With the bulk ^{3}He present we could only say that the ^{3}He signal was diminished within no more than 10 sec after the ^{19}F was fully saturated.

An additional surprise arose from some measurements made on the ^{3}He T_1 under conditions of substrate saturation. Ordinarily, the short T_1

values observed for ^{3}He in restricted geometries are attributed to heightened relaxation at the walls. Following a 90° pulse on the ^{3}He (so that $M = 0$ throughout the sample), this heightened wall relaxation is thought to act as a magnetization source that returns the entire sample to the M_0 value characterizing thermal equilibrium. But with the polarization for the surface ^{3}He diminished as a result of the ^{19}F saturation, it is evident that the surface may no longer act as a source of magnetization. Indeed, when the magnetization at the surface is less than that in the bulk, the surface instead appears as a magnetization sink rather than source. The saturation condition of the substrate spins might therefore be thought of as a means for decoupling the ^{3}He bulk from the wall relaxation processes. This expectation, however, proved to be in error.

Figure 12 displays two ^{3}He recovery curves plotted in the standard manner so that the T_1 is given by the slope of the lines. The closed circles in the upper curve record the recovery of the entire ^{3}He sample with the substrate and surroundings in thermal equilibrium (i.e., the ^{19}F spins were not being saturated). These data indicate a T_1 of approximately 10 sec. The ^{3}He signal was then reduced by the aforesaid 35% via ^{19}F saturation, and the T_1 again measured for this remaining signal. The open circles in the lower curve show that the ^{3}He T_1 in the two instances did not differ. Although the curves are displaced due to the signal reduction following ^{19}F saturation, the slope for the open circles is not at all close to that typical of T_1 values for bulk ^{3}He (at least 10^2 sec). Instead, the recorded T_1 appears to remain at the same surface-dominated value seen in the upper curve. This observation is difficult to understand using the simple picture outlined in the preceding paragraph. For, if the surface relaxation for the ^{3}He occurred only at the interface between the ^{3}He and substrate, the ^{19}F saturation would be expected to decouple the ^{3}He from such processes with much the same effect as a ^{4}He preplating.

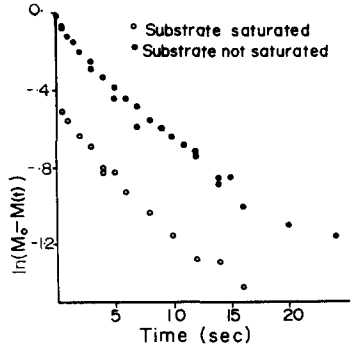

Fig. 12. Recovery curves for ^{3}He measured before (solid circles) and during (open circles) ^{19}F saturation. Although the ^{19}F saturation does result in a decreased ^{3}He signal, the T_1 time constant appears to be unchanged.

The overall behavior of the ^{3}He T_1 nonetheless points to the surface region as the means for relaxation. Recall that for a single ^{3}He layer the measured T_1 was only 200 msec, although this was interpreted as the time for communication with the ^{19}F spins (Section 3.1). However, even the inferred time constant for direct relaxation (~3 sec) was still shorter than the 10 sec measured for the experiments of this section, where bulk ^{3}He filled the pores. In fact, as the amount of ^{3}He in the cell was increased from a monolayer to full pore capacity, the measured ^{3}He T_1 rose from 200 msec to the 10 sec seen in Fig. 12. This qualitatively fits the model in which the higher layers of ^{3}He depend somehow on the surface for relaxation. The addition of ^{3}He sample filling regions far from the surface may thus be seen to result in an overall increase in the measured T_1 since such additions merely burden the efficient centers with more spins to relax. In addition, we have already noted that the T_1 time scale recorded in these experiments is far shorter than bulk values, so a surface role is the natural culprit to suspect.

There are additional questions raised by just the time scale of the T_1 values in Fig. 12. We have modeled the relaxation pathway for both the ^{19}F and ^{3}He according to the scheme in Fig. 13. Since the surface spin reservoirs are pictured as the strongest link to the lattice, both the ^{3}He and ^{19}F would have to ultimately rely on the same bottlenecked steps in order to relax. Following a saturation of either spin species, the bulk magnetization would be refreshed as the small surface reservoirs trickled heat into the colder thermal lattice. In addition, with ^{3}He filling in the pores, the size of the two bulk reservoirs would be comparable. This picture, then, would imply that the bulk ^{3}He and ^{19}F relax at comparable rates so long as both

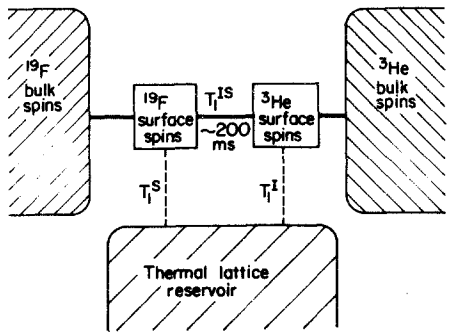

Fig. 13. Reservoirs communicating during a ^{3}He or ^{19}F recovery. If both the ^{19}F and ^{3}He equilibrium rates were limited by the surface bottleneck, the T_1 values for the two species would be comparable.

processes involve the surface bottleneck (which we know to be the case for at least the ^{19}F). Since the ^{3}He relaxation rates are observed to exceed those for the ^{19}F by a factor of 10, we need significant additions to this simple picture. There must in fact be additional relaxation mechanisms for the bulk ^{3}He that are not available to the ^{19}F. Note that this is similar to the situation we faced when confronted with the two T_1 values in Fig. 12. For, with the pathway for surface relaxation supposedly eliminated, the bulk ^{3}He was still able to maintain a short T_1. Hence, we were left searching for possible ^{3}He relaxation mechanisms apart from those confined to the ^{19}F–^{3}He interface.

In contrast to the questions raised above, one conclusion may be drawn from these data. A worry concerning the approach followed in the present study could have been that the very strong coupling between the ^{3}He and ^{19}F spins might dominate even the bulk ^{3}He relaxation in a manner not typical of other substrates. With an easy exchange of magnetization occurring between the ^{3}He and ^{19}F at the boundary, one might suspect that the short time recovery measured in a ^{3}He T_1 arose merely from the refreshing effect of the substrate magnetization. But we now see that this is not the case. We have already pointed out that large changes in the substrate T_1 (induced through oxygen addition) had no effect on the ^{3}He. In this section we have seen in addition that when the substrate spins were saturated, there was still no effect on the ^{3}He T_1. This is somewhat comforting, in the sense that the presence of the substrate spin magnetization cannot be thought to dominate the ^{3}He relaxation behavior. There must instead be other features about the surface that are responsible for the ^{3}He relaxation. The ^{19}F data then offer a clean probe of the surface, and the questions raised in this and the preceding sections should be relevant for ^{3}He relaxation in other confined geometry experiments.

4. SUMMARY

The present work has employed a fluorocarbon substrate for a study of ^{3}He properties in a confined geometry. By monitoring both the ^{19}F and ^{3}He spin species we observe a nuclear interaction at the walls that allows the easy transfer of magnetization between these two spin baths. Experiments performed after preplating the surface with a ^{4}He monolayer reveal that the nuclear interaction is short ranged.

The link between the two spin baths opens up the surface ^{3}He relaxation channels to the substrate ^{19}F. Consequently, the relaxation time of the bulk ^{19}F spins is quite sensitive to the presence of ^{3}He on the surface. Adsorbing a monolayer of ^{3}He on the surface increases the ^{19}F $1/T_1$ by a factor of 10; intermediate coverages show structure in the ^{19}F relaxation rates that

identifies aspects important in the surface ^{3}He link to the lattice reservoir. The ^{19}F–^{3}He spin bath link is seen to result in a saturation of the monolayer ^{3}He signal whenever the ^{19}F spins are directly saturated by rf irradiation. With bulk ^{3}He present, ^{19}F saturation results in a diminished ^{3}He signal.

TABLE I

The ^{19}F Relaxation Time T_1 with Various ^{3}He Coverages and Temperatures[a]

	T_1 and ^{3}He coverage								
He^3 in cell, μ mol	0.4 K	0.8 K	1.2 K	1.6 K	2.0 K	2.4 K	2.7 K	3.1 K	3.7 K
0	7950	2940	1370	933	661	474	388	314	211
	0	0	0	0	0	0	0	0	0
45	5930	2020	1090	694	480	322	249	191	122
	1.22	1.22	1.22	1.22	1.22	1.22	1.22	1.22	1.22
85	486	277	227	192	165	117	96.3	76.1	61.1
	2.31	2.31	2.31	2.31	2.31	2.31	2.31	2.31	2.31
101	205	162	149	130	109	86.9	75.8	67.1	59.5
	2.75	2.75	2.75	2.75	2.75	2.75	2.75	2.75	2.75
108	159	139	134	106	93.2	76.2	71.0	62.9	55.0
	2.95	2.95	2.95	2.95	2.95	2.95	2.95	2.95	2.95
116	141	130	111	98.9	83.6	68.5	65.0	60.7	58.0
	3.16	3.16	3.16	3.16	3.16	3.16	3.16	3.16	3.16
124	135	123	108	90.7	75.8	62.6	59.0	55.3	52.8
	3.38	3.38	3.38	3.38	3.38	3.38	3.38	3.38	3.38
132	—	131	115	93.7	75.7	60.6	56.1	52.1	50.6
	—	3.61	3.61	3.61	3.61	3.61	3.61	3.61	3.61
140	162	140	128	101	84.4	62.9	56.6	51.5	46.1
	3.82	3.82	3.82	3.82	3.82	3.82	3.82	3.82	3.82
149	175	155	138	117	96.0	69.6	61.0	51.8	46.9
	4.05	4.05	4.05	4.05	4.05	4.05	4.05	4.05	4.05
160	135	118	104	88.2	78.6	68.5	64.3	58.3	51.2
	4.36	4.36	4.36	4.36	4.36	4.36	4.36	4.35	4.30
176	90.5	89.0	91.1	86.5	82.5	74.7	66.8	63.4	52.9
	4.79	4.79	4.79	4.79	4.79	4.79	4.77	4.72	4.58
191	89.8	87.3	92.4	87.9	83.3	76.0	73.6	63.4	52.7
	5.21	5.21	5.21	5.21	5.21	5.18	5.13	5.04	4.81
208	95.5	101	104	97.7	88.4	78.9	69.9	63.6	53.6
	5.66	5.66	5.66	5.66	5.64	5.56	5.48	5.34	5.02
222	113	123	115	103	100	78.8	73.4	66.7	52.3
	6.06	6.06	6.06	6.03	6.00	5.86	5.74	5.56	5.19
237	129	128	120	105	90.8	78.7	73.1	67.0	55.0
	6.48	6.48	6.48	6.43	6.34	6.12	5.97	5.76	5.31
268	148	144	134	105	92.1	80.7	73.1	64.5	56.6
	7.32	7.32	7.24	7.10	6.81	6.44	6.21	5.93	5.38

[a]The experiment was performed with a resonant frequency of 10 MHz for the ^{19}F nuclei. Each position in the matrix shown in the table contains two numbers. The upper number is the measured value of T_1 in seconds. The lower number is the ^{3}He coverage in STP cm^3 of ^{3}He per gram of DLX6000.

This shows that the wall disturbance is also important in the interstitial bulk region. Curiously, ^{19}F saturation does not affect the T_1 of the bulk ^{3}He spins.

ACKNOWLEDGMENTS

The authors are grateful to Maurice Chapellier for stimulating discussions on this subject. The research was supported by the Cornell Materials Science Center through NSF Grant DMR 8217227 and by a contract from the Office of Naval Research.

APPENDIX

Figure 9 shows how the ^{19}F coverage features change with temperature. In Table I we list the data from these various temperature runs taken at $H_0 = 2.5$ kG.

REFERENCES

1. W. M. Fairbank and G. K. Walters, in *Proceedings of Symposium on Liquid and Solid ^{3}He* (Ohio State University, 1957).
2. R. L. Garwin and H. A. Reich, *Phys. Rev.* **115**, 1478 (1959).
3. G. Careri, I. Modena, and M. Santini, *Nuovo Cimento* **13**, 1779 (1959).
4. P. Monod and J. A. Cowen, Service di Physique du Solide et Resonance Magnetique, Centre D'Etudes Nucleaires de Saclay, Technical Report (1967), unpublished.
5. D. F. Brewer, D. J. Creswell, T. Goto, M. G. Richards, J. Rolt, and A. L. Thomson, in *Monolayer and Submonolayer Helium Films* (Proc. Symp. Hoboken, New Jersey, 1973).
6. J. Kelly, Ph.D. Thesis, Cornell University (1974), unpublished.
7. H. Godfrin, G. Frossati, D. Thoulouze, M. Chapellier, and W. G. Clark, *J. Phys. (Paris)* **39** (Suppl. 8), C6-287 (1978).
8. B. P. Cowan, *J. Low Temp. Phys.* **50**, 135 (1983).
9. R. C. Albers, Ph.D. Thesis, Cornell University (1977).
10. R. C. Albers and J. W. Wilkins, *J. Low Temp. Phys.* **34**, 105 (1979).
11. M. T. Beal-Monod and D. L. Mills, *J. Low Temp. Phys.* **30**, 289 (1978).
12. J. C. Wheatley, *Phys. Rev.* **165**, 304 (1968).
13. A. J. Leggett and M. Vuorio, *J. Low Temp. Phys.* **3**, 359 (1970).
14. R. A. Guyer, *J. Low Temp. Phys.* **10**, 157 (1973).
15. D. L. Mills and M. T. Beal-Monod, *Phys. Rev. A* **10**, 343 (1974).
16. D. L. Mills and M. T. Beal-Monod, *Phys. Rev. A* **10**, 2473 (1974).
17. J. P. Harrison, *J. Low Temp. Phys.* **37**, 467 (1979).
18. J. V. Gates and W. H. Potter, *Phys. Rev. B* **13**, 8 (1976).
19. L. J. Friedman, P. Millet and R. C. Richardson, *Physica* **108B**, 837 (1981).
20. L. J. Friedman, Ph.D. Thesis Cornell University (1983).
21. L. J. Friedman, P. Millet and R. C. Richardson, *Phys. Rev. Lett.* **47**, 1078 (1981).
22. Y. Goto, Ph.D. Thesis, University of Sussex (1977).
23. M. Chapellier, *J. Phys. Lett. (Paris)* **43**, 1609 (1982).
24. P. C. Hammel, L. J. Friedman, T. Mamiya and R. C. Richardson, *Bull. Am. Phys. Soc.* **28**, 675 (1983).
25. M. Chapellier, *Bull. Am. Phys. Soc.* **28**, 357 (1983).
26. H. Ramm, P. Pedroni, J. Thompson and H. Meyer, *J. Low Temp. Phys.* **2**, 539 (1970).
27. S. Brunauer, P. H. Emmett, and E. Teller, *J. Am. Chem. Soc.* **60**, 309 (1938)